

Reordering of magnetic colloid structures in external magnetic fields

André Heinemann,* Albrecht Wiedenmann and Martin Kammel

Hahn-Meitner-Institut Berlin, Glienicker Strasse 100, D-14109 Berlin, Germany. Correspondence e-mail: heinemann@hmi.de

Field-induced local ordering within a cobalt-based magnetic colloid has been studied with polarized small-angle scattering by turning the direction of the external magnetic field. By analysing the nuclear–magnetic cross term we were able to separate the scattering contributions from dipolar chains and domains of pseudo-crystalline hexagonal arrangements. The magnetic moments were found to be aligned along the external magnetic field and to follow the change of the field direction. The observed variation of the particle moments must give rise to a rearrangement of the local hexagonal structure with respect to the new field direction to explain the scattering pattern. We confirm this by two-dimensional simultaneous least-squares fits for different Q ranges [where $Q = 4\pi \sin(\theta)/\lambda$, λ is the X-ray wavelength and 2θ is the scattering angle] with a model containing a core–shell particle form factor and a structure factor composed of Gaussian peaks and contributions from polydisperse cylinders.

© 2007 International Union of Crystallography
Printed in Singapore – all rights reserved

1. Motivation and experimental setup

Small-angle neutron scattering with polarized neutrons (SANS POL) is an excellent tool to obtain insights into the inherent and magnetic field-induced nanostructure of magnetic liquids (Wiedenmann *et al.*, 2003). In some concentrated Co-based ferrofluids, well defined peaks appeared in the two-dimensional scattering pattern which have been assigned to a local pseudo-crystalline hexagonal ordering (see Fig. 1). In Wiedenmann *et al.* (2003), the observed SANS pattern is interpreted as an arrangement of nanometre-sized core–shell particles in hexagonal planes where the magnetic moments are aligned along the external field \mathbf{H}_{ext} direction. Furthermore, in other samples (Wiedenmann & Heinemann, 2005), the possible coexistence of hexagonal ordered domains with segments of dipolar chains can explain the observed scattering patterns. When the strength of the

external magnetic field \mathbf{H}_{ext} was increased, this model applied to the experimental data leads to the conclusion of a continuous transition from chain-like aggregates to layered structures. This interpretation, based on common SANS and SAXS experiments, is not unique. We have tried to eliminate some of the ambiguities by a magnetic field-direction variation study. It was not clear whether the local particle ordering is conserved while the magnetic moments follow the change in the external field, or if reordering of the particles occurs in a new structure defined by the new field direction.

A horizontal magnet was installed on a turntable to vary the angle between the incoming neutron beam and the external field \mathbf{H}_{ext} , both spanning a plane perpendicular to the detector. By turning the magnet (Ω rotation), both the field and the sample change their orientations with respect to the neutron beam. The sample, a Co-based magnetic liquid, MFT3 (the same as used in Wiedenmann & Heinemann, 2005), with mean particle core radius $R = 4.4$ nm coated by a layer ($D = 1.9$ nm) of oleoylsarkosine as surfactant and dispersed in an oil, L9, could be rotated independently (ϕ rotation). We performed three combinations of these rotational degrees of freedom and analysed the two-dimensional scattering pattern, taking into account all influences of the varying orientation between the \mathbf{Q} vector [$Q = 4\pi \sin(\theta)/\lambda$, with the X-ray wavelength λ and the scattering angle 2θ] and \mathbf{H}_{ext} .

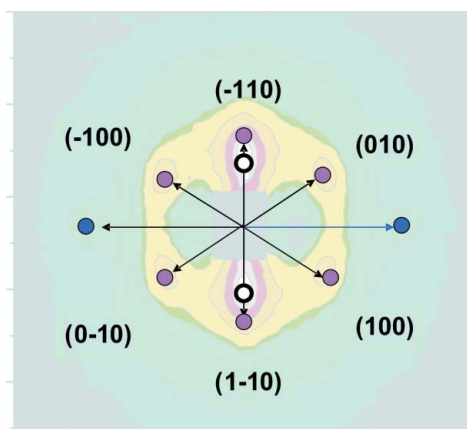


Figure 1

Correlation peaks as observed in concentrated Co ferrofluid (Wiedenmann *et al.*, 2003), with \mathbf{H}_{ext} horizontal and perpendicular to the incident neutrons. In-plane peaks indexed in hexagonal symmetry. The vertical extra peaks (001) correspond to the inter-plane spacing.

2. Two-dimensional SANS and SANSPOL analysis

In this type of experiment, the change in the external magnetic field \mathbf{H}_{ext} , which likewise defines the neutron spin direction, has different influences on the scattering pattern. Generally, only the magnetic contrast perpendicular to the \mathbf{Q} vector contributes to the coherent scattering. A change in the external \mathbf{H}_{ext} direction may generate a change in the local magnetization direction and so in the magnetic contribution to the total scattering. For a dilute system of particles with neither permanent nor induced interparticle correlations, this can be incorporated using an adapted $\sin^2 \alpha$ law. Anisotropic

magnetic structures with a local magnetization direction \mathbf{M} and symmetry axis or axis of preference lead to a more complicated dependence of the scattering cross section from the interplay of this axis with \mathbf{Q} , \mathbf{H}_{ext} and \mathbf{M} . In the following, we use the definitions shown in Fig. 2. For instance, in order to observe contributions from Bragg-like scattering of magnetic correlations, it is not only necessary that the correlation direction is within the detector plane, but also that it must have a non-vanishing component perpendicular to the respective \mathbf{Q} vector represented by a detector cell. When polarized neutrons are used to investigate anisotropic magnetic structures, the situation is even more complex. Here, a possible divergence of the local magnetization \mathbf{M} and the external magnetic field \mathbf{H}_{ext} can lead to additional variations in the SANS POL intensities.

2.1. SANS POL for uncorrelated systems

For a polarized neutron beam, let P denote the degree of polarization and ε the spin-flipper efficiency. If the polarization of the scattered neutrons is not analysed, one can distinguish between I^+ and I^- scattering by switching a spin flipper in front of the sample on and off. Here (see *e.g.* Heinemann & Wiedenmann, 2003), I^+ evaluates to:

$$I(Q)^+ \propto (F_N)^2 + (F_{\mathbf{M}\perp\mathbf{Q}})^2 + 2P(2\varepsilon-1)F_N(F_{\mathbf{M}\perp\mathbf{Q}})_z. \quad (1)$$

The \mathbf{z} or spin direction is defined by the external field (F_N is the nuclear scattering amplitude and F_M is the magnetic scattering amplitude). Thus, it appears that the interference term in equation (1) depends on the relative orientations of \mathbf{H}_{ext} , \mathbf{M} and \mathbf{Q} , whereas the second term in equation (1) is identical to the magnetic scattering for non-polarized neutrons and is affected only by the angle between \mathbf{M} and \mathbf{Q} . We will focus here on the result that a deviation of the local magnetization direction from the external field direction is at least detectable *via* the interference term using polarized neutrons. For superparamagnetic particles, such as for the nanosized core-shell particles in magnetic fluids used in our experiment, equation (1) evaluates to:

$$I^+ = \int dR N(R) \left\{ F_N^2 + \frac{2F_M^2 L_\beta}{\beta} + \left(F_M^2 - \frac{3F_M^2 L_\beta}{\beta} \right) \left[1 - \left(\frac{\mathbf{M} \cdot \mathbf{Q}}{MQ} \right)^2 \right] + 2P(2\varepsilon-1)F_N F_M L_\beta \left(\frac{\mathbf{M} \cdot \mathbf{H}}{MH} - \frac{\mathbf{M} \cdot \mathbf{Q}}{MQ} \frac{\mathbf{H} \cdot \mathbf{Q}}{HQ} \right) \right\}. \quad (2)$$

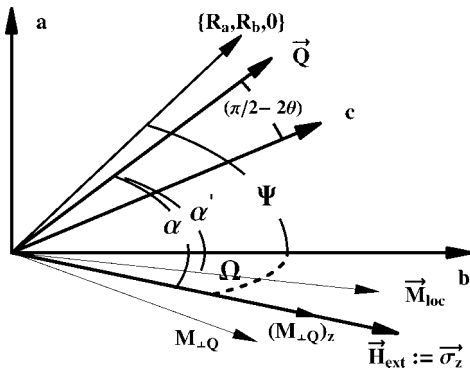


Figure 2
The detector plane $\mathbf{a} - \mathbf{b}$ and the neutron beam direction \mathbf{c} . The predefinition of $\mathbf{H}_{\text{ext}} = H\mathbf{z}/z$ fixes the meaning of the angles α , Ψ and Ω . 2θ is the scattering angle, with $Q\lambda = 4\pi \sin \theta$ and $\mathbf{Q} = \{\cos \theta \cos \Psi, \cos \theta \sin \Psi, -\sin \theta\}$.

I^- is obtained from equation (2) for $\varepsilon = 0$. $L_\beta = \coth(\beta) - 1/\beta$ is the Langevin function, with $\beta = \mu_0 \mathbf{H} \cdot \mathbf{M}/k_B T$ (k_B is Boltzmann's constant and T is temperature). Using the definitions in Fig. 2, the cross term (intensity difference) reads

$$I^+ - I^- = 4P\varepsilon F_N F_M L_\beta [\cos \angle(\mathbf{M}, \mathbf{H}_{\text{ext}}) - \cos \alpha \cos \alpha']. \quad (3)$$

In the special case where \mathbf{M} is aligned along \mathbf{H}_{ext} , equation (3) is simplified to:

$$I^+ - I^- = 4P\varepsilon F_N(Q) F_M(Q) L_\beta \sin^2 \alpha. \quad (4)$$

2.1.1. Inter-particle correlations: the structure factor $S(\mathbf{Q})$. Inter-particle correlations are commonly taken into account in SANS cross sections by a structure factor $S(\mathbf{Q})$. This general approximation is based on the splitting of the total intensity into contributions from isolated scatterers and from inter-particle interference using different types of approach (Pedersen, 1994). We compare the results from a local monodisperse model,

$$I(\mathbf{Q}, \Psi) \propto \langle F(Q)^2 \rangle \langle S(Q, \Psi) \rangle, \quad (5)$$

and a decoupling model based on

$$I(\mathbf{Q}, \Psi) \propto \langle F(Q)^2 \rangle + [\langle F(Q) \rangle]^2 [S(Q, \Psi) - 1], \quad (6)$$

and find no significant differences in the data fitting procedure. Thus, we present the results from the simpler local monodisperse approximation. In equations (5) and (6), $\langle \dots \rangle = \int N(R) \dots dR$ is an abbreviation for the squared amplitude average and the amplitude average itself over the particle size distribution $N(R)$. For the form factor $F(Q)$, we used a polydisperse core-shell model, which was very successful for parameter determination of dilute samples [see *e.g.* Heinemann & Wiedenmann (2003) and references therein].

The model for the structure factor $S(\mathbf{Q})$ is composed of two different contributions. The Bragg-like peaks from the pseudo-crystalline structure are described by a Gaussian profile of the form

$$S_{hkl}(\mathbf{Q}) \propto 1 + I_{\text{max}} \exp \left[-\frac{4(\mathbf{Q} - \mathbf{Q}_{hkl})^2}{\pi \Delta_{hkl}^2} \right], \quad (7)$$

where the \mathbf{Q}_{hkl} define the peak positions and Δ_{hkl} the related peak widths. After correction for instrumental resolution, the widths are correlated to the mean sizes of the ordered domains by the Debye-Scherrer equation $L = 2\pi/\Delta_{hkl}$. The second contribution describes the scattering at low Q values, which dominates the two-dimensional images for the sample-detector (SD) distance at 12 m (low Q range) and which shows the typical scattering pattern of long but small objects aligned along the field direction. We model this contribution as a structure factor constructed of polydisperse cylinder scattering amplitudes (Guinier & Fournet, 1955) *via*

$$\langle S_{\text{cyl}} \rangle = [1 - N_{\text{cyl}} \langle F_{\text{cyl}}(Q, Q_{\parallel}) \rangle]^{-1}, \quad (8)$$

with

$$\langle F_{\text{cyl}} \rangle \propto \iint dN_L dN_R \frac{4\pi R}{Q_{\perp} Q_{\parallel}} J_1(RQ_{\perp}) \sin \left(\frac{Q_{\parallel} L}{2} \right), \quad (9)$$

where dN_L and dN_R indicate integration over the normalized length and radius distributions. $J_1(z)$ is the first-order Bessel function, and Q_{\parallel} and Q_{\perp} are the moduli of the scattering vector parallel and perpendicular to the orientation axis, respectively. This non-unique choice turned out to be the simplest model with the capability of reflecting the observed scattering pattern for small Q values. Two-dimensional fitting with this double integral in equation (9) is very time consuming and not practicable. With the assumption of a gamma-type size distribution (Heinemann *et al.*, 2000) for the radius

Table 1

Mean values and limits of the 95% confidence intervals for the least-squares fit of SANSPOLE data from the concentrated Co-based ferrofluid.

The magnetic scattering contrast for $\mu_0 H = 1$ T was fixed to the cobalt bulk value of $4.14 \times 10^{14} \text{ m}^{-2}$. For the dilute sample, one obtains for the mean particle radius $\mu = 44$ nm and for the shell thickness $d = 19$ nm. η_∞ , η_{Co} and η_{shell} are the neutron nuclear scattering contrasts for the matrix, the shell and the Co core, respectively.

Fitted	μ (nm)	σ (nm)	d (nm)	η_∞ ($\times 10^{14} \text{ m}^{-2}$)	Vol. %
Mean	5.0	0.9	1.9	1.3	4.9
Error	0.7	0.2	0.3	0.4	0.2

Fixed	P	ε	$L(\beta)$	η_{Co} ($\times 10^{14} \text{ m}^{-2}$)	η_{shell} ($\times 10^{14} \text{ m}^{-2}$)
Value	0.93	0.98	1	2.53	0.33

Table 2

Fit results for the structure factor parameters.

These values are obtained by a simultaneous fit of the single-particle properties and the inter-particle correlations at SD = 4 m and SD = 12 m.

R (nm)	σR (nm)	L (nm)	σL (nm)	Q_{100} (nm^{-1})	Δ_{100} (nm^{-1})
4.7	1.3	35.4	4.2	0.39	0.062

and an independent cylinder-length size distribution of the same type, we obtained an analytical result for $\langle F_{\text{cyl}} \rangle$ in equation (9):

$$\langle F_{\text{cyl}} \rangle = \frac{2}{Q_{\parallel}} \left(\frac{Q_{\parallel}^2 \sigma L^4}{4L^2} + 1 \right)^{-L^2/2\sigma L^2} \pi(\sigma R^2 + R^2) \times \text{H2F1} \left[\frac{R^2}{2\sigma R^2} + 1, \frac{1}{2} \left(\frac{R^2}{\sigma R^2} + 3 \right); 2; \frac{(Q_{\parallel}^2 - Q^2)\sigma R^4}{R^2} \right] \times \sin \left[\frac{L^2 \cot^{-1}(2L/Q_{\parallel}\sigma L^2)}{\sigma L^2} \right], \quad (10)$$

where H2F1 is an abbreviation for the hypergeometric function ${}_2F_1(a, b; c; z) = \sum_{k=0}^{\infty} (a)_k (b)_k / (c)_k z^k / k!$ (see e.g. Weisstein, 1999), L is the mean cylinder length and σL its standard deviation, and R is the mean radius and σR its standard deviation. In this approach the distributions for the radii and lengths of the cylinders are totally decoupled. To exclude parameter correlations in the least-squares fit as far as possible, we applied constraints to the parameters. For instance, the mean cylinder radius and the mean single-particle radius are connected to vary in the same direction during the fit.

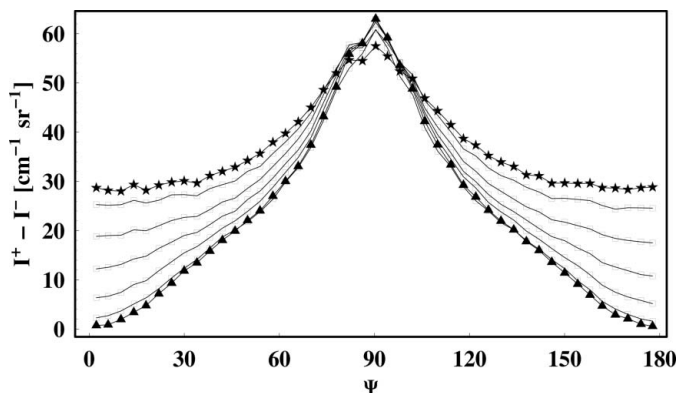


Figure 3
 $I^+ - I^-$ for different magnetic field directions Ω ($^\circ$) = 0 (closed triangles), 10, 20, 30, 40, 50, 60 (closed stars) (from bottom to top) at $Q = 0.39 \text{ nm}^{-1}$ versus the angle Ψ between \mathbf{Q} and the detector b axis.

3. Experimental results

The following discussion will reveal possible traps during a straightforward interpretation of the scattering pattern obtained and shows ways out of these. As mentioned in §2.1, only the magnetic component perpendicular to \mathbf{Q} leads to a scattering contribution. If we turn the magnetic field with respect to the fixed detector, identical detector cells $\{R_a, R_b, 0\}$ defining a special \mathbf{Q} vector collect different magnetic scattering contributions even without any change in the sample structure. The strong influence of this effect is illustrated in Fig. 3. This seems to suggest that by turning the magnetic field the scattering intensity for detector cells at small angles with respect to the b axis increases, but the reason is that equal cells now collect different magnetic scattering contributions. The implication of this effect is clearly demonstrated by re-scaling the intensities with the change of the magnetic contribution ($\propto \sin^2 \alpha$) and plotting the intensities versus Ψ , now assuming that the moment direction of the particles corresponds to the direction of the external field. If the particle arrangement were still the same at any angle Ω , the scaling of the intensities in Fig. 3 by $\sin^2 \alpha$ should lead to one single master curve for all values of Ω . The re-scaled intensities in Fig. 4 show that this is obviously not the case. While the central peak at 90° is not affected by the Ω tilting, clear differences appear at $\Psi = 30$ and 150° , corresponding to the hexagonal peaks. It is now evident that the intensity is not only influenced by the direction of the magnetic moment but also by a reordering of the particles. Fig. 4 shows clearly that by turning the external magnetic field the detector image cannot provide us with complete information about the anisotropic angle dependence of the magnetic scattering. This kind of processing and presentation of the data gives good insights into the possible changes of a structure factor which follows directly the magnetic field direction, like the S_{cyl} in our model, while for S_{hkl} it does not. The reason is that the appearance of peaks in the detector is a result of fulfilling the Laue conditions for a special \mathbf{Q} vector. This leads to the Q - and Ψ -dependence of P_{hkl} in equation (7), whereas F_{cyl} , which defines S_{cyl} by equation (8), depends on α via $Q_{\parallel} = Q \cos \alpha$.

It is obvious that a one-dimensional presentation of the data can hardly show all aspects of the influence of the magnetic field direction on the different anisotropic structure factors. For the same reason, one-dimensional data fitting methods will show application limitations here. Besides the different angle dependence of the two structure factors, they have different strong influences on the total

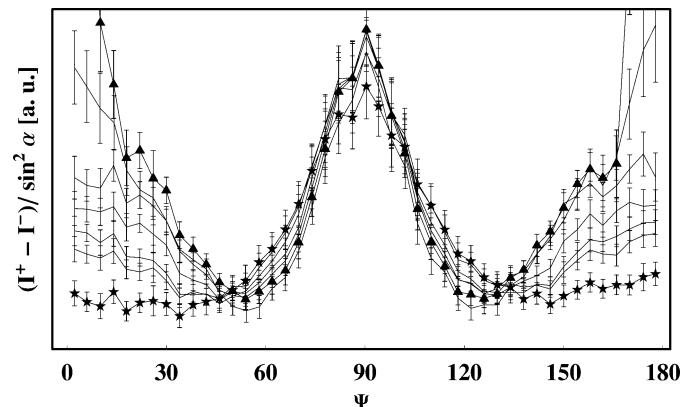


Figure 4
 $(I^+ - I^-) / \sin^2 \alpha$ for different magnetic field directions Ω ($^\circ$) = 0 (closed triangles), 10, 20, 30, 40, 50, 60 (closed stars) (from top to bottom) at $Q = 0.39 \text{ nm}^{-1}$, showing the disappearance of the hexagonal peaks with increasing Ω . a.u. = arbitrary units.

scattering for different Q ranges, *i.e.* different sample–detector distances. This forces us to apply a two-dimensional data-fitting method with simultaneous fitting of the SD = 4 m and SD = 12 m experimental results. By doing this we obtain not only parameter values for the single particles, but also very reasonable values for the structure factor parameters (see Table 2). Within the error bars, the parameters describing the single particles are the same as obtained by fitting experimental results from dilute samples of the same type (see Table 1) fitted using a different program. Figs. 5 and 6 show comparisons of the experimental data and the simultaneous fitting results of the complete set of parameters as presented in Tables 1 and 2. In Fig. 6, only the influence of the cylindrical structure factor is relevant to explain the data. We assume that this structure factor represents the influence of chain-like structures in the ferrofluid, giving rise to low- Q anisotropic scattering. In Fig. 5, we observe an interplay between the assumed hexagonal pseudo-crystalline structure and the chain-like correlations. It was essential to apply a simultaneous fit to the two different Q ranges, otherwise the procedure runs into local minima for the SD = 4 m data which cannot explain the SD = 12 m data.

4. Influences of the H field direction

After obtaining the parameter values for the single particles and the structure factors for the $\Omega = 0^\circ$ case, we study the influence of the change of the magnetic field direction on the structure. As long as our model of chain-like structures represented by cylindrical structure factors is applicable and the chains follow a change of the magnetic field direction, the influence on S_{cyl} is well known by substituting $Q_{\parallel} = Q \cos \alpha$ in equation (10). Now we look at the contribution from the field-induced hexagonal pseudo-crystalline structure, which was found to disappear in zero field. If we assume that the particle ordering itself follows the direction of the external magnetic field, the Laue conditions for the reciprocal pseudo-lattice vectors are no longer fulfilled for the Q vectors within the detector plane. For long-range ordered structures, δ -like peaks would disappear instantaneously by turning Ω , and hence the reciprocal lattice, out of the detector plane. For real peaks broadened by the finite size of the ordered domains, the observed intensity is the result of a convolution of the peak width with the Ewald-sphere conditions. The main effect of the convolution must result in a decrease of the peak height, since only part of the full two-dimensional peak is cut off in the detector

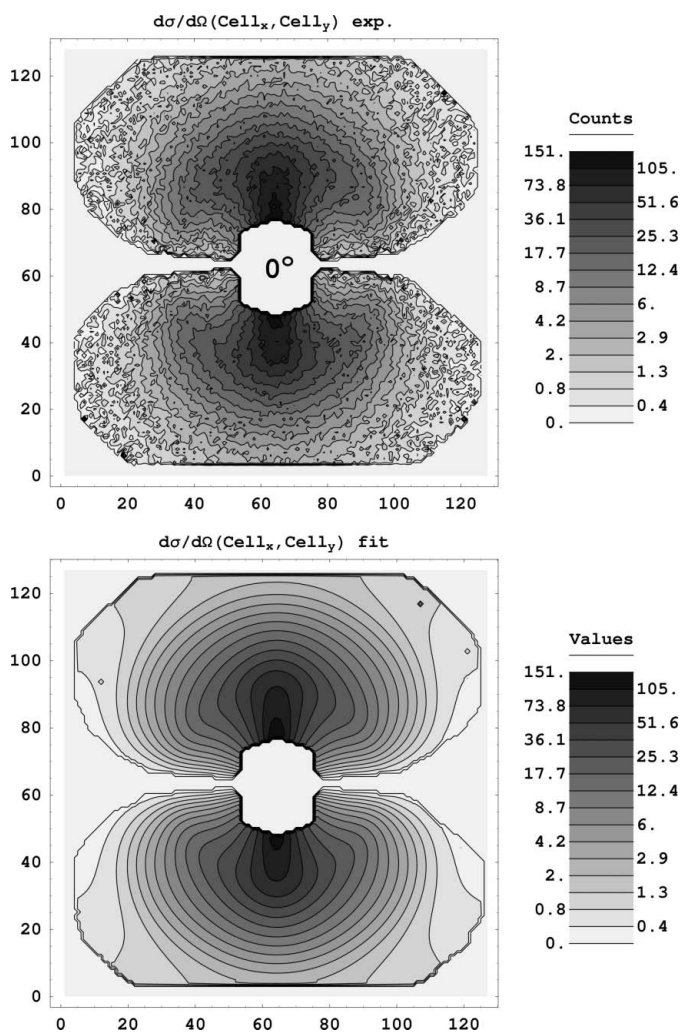


Figure 5 Two-dimensional scattering pattern $I^+ - I^-$. Experimental data (top) and fit results (bottom) for SD = 4 m and $\Omega = 0^\circ$.

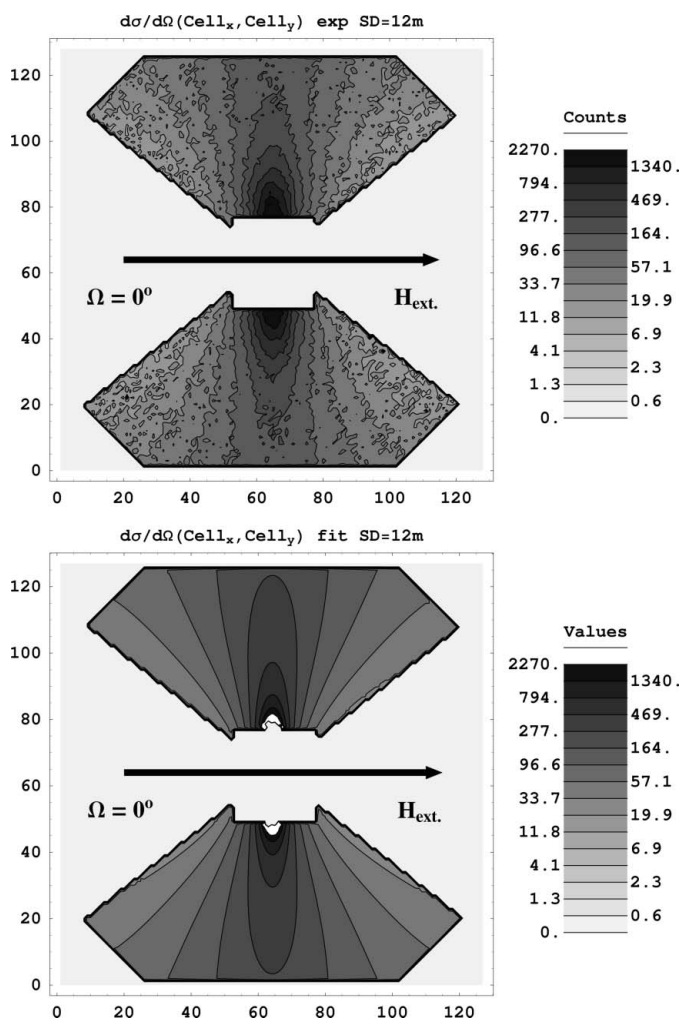


Figure 6 Two-dimensional scattering pattern $I^+ - I^-$. Experimental data (top) and fit results (bottom) for SD = 12 m and $\Omega = 0^\circ$.

Table 3

Results for the hexagonal peak intensities progression depending on the field direction Ω .

These values are obtained by fixing all other parameters to the results from the $\Omega = 0^\circ$ fit.

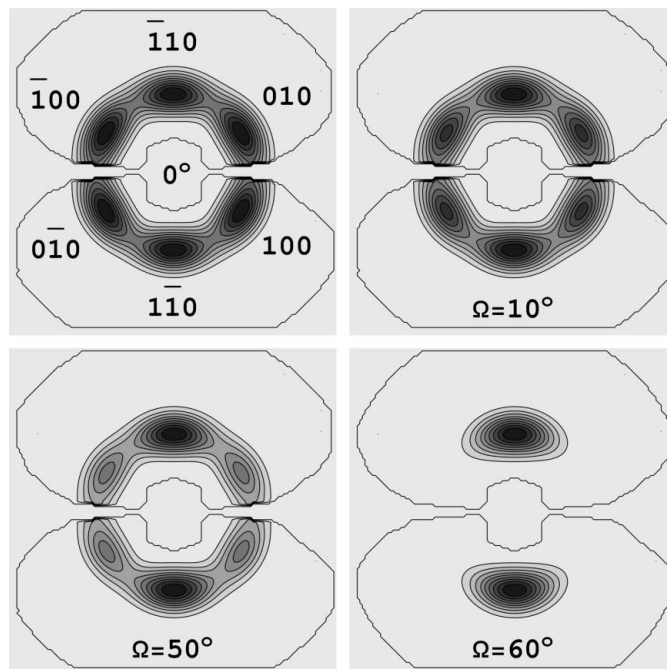
Ω ($^\circ$)	0	10	20	30	40	50	60
$I_{\max}/I_{\max}(\Omega = 0)$	1	0.8	0.83	0.78	0.69	0.51	< 0.01

plane when Ω is increased from 0° . Due to the large polydispersity, no change of the observed positions and widths of the peaks could be detected. The width of the peaks in $\Delta\Phi$ and ΔQ was fixed to the value obtained at $\Omega = 0$. Therefore, in a simultaneous fit of all data for the different \mathbf{H}_{ext} directions, we fixed all structure parameters and fitted only the height of the 100, $\bar{1}00$, 010 and $0\bar{1}0$ hexagonal peaks. Because the change of the magnetic field direction will not affect the symmetry for the $\bar{1}10$ and $1\bar{1}0$ peaks, this contribution is fixed too.

Fig. 7 shows the S_{hkl} part of the fits for different orientations of the magnetic field. A rotation $\Omega = 10^\circ$ of the magnetic field with respect to the detector plane leads to a significant drop in intensity at the peak positions mentioned above. The loss of intensity continues by turning the H field more and more in the neutron beam direction (see Table 3). After reaching $\Omega = 60^\circ$, there is no longer any evidence of these peaks in the fit. This behaviour clearly shows that both the nuclear and magnetic ordering are induced by the magnetic field. The particle arrangement in hexagonal layers is fully determined by the direction of the external magnetic field, as well as by the moment direction of the particles.

5. Conclusions

By turning the direction of the magnetic field, we were able to separate consistently with our model the scattering contributions resulting from dipolar chains and those from domains of pseudo-crystalline hexagonal arrangements. An arrangement of particles in chain-like structures is manifested by explaining the data with a cylindrical structure factor. We also obtained values for the length of these chains of about 35 ± 4 nm. The thickness fits well to the single-particle properties, as shown in Table 1. The simultaneous fits of the two-dimensional patterns are consistent with the picture of local hexagonal ordering of the nanoparticles induced by the external magnetic field. The results show unambiguously that the magnetic moments are aligned along the external magnetic field. This re-orientation of the particle moments along the new direction of \mathbf{H}_{ext} must give rise to a rearrangement of the local structure with respect to the new field direction. The correlation length of the ordered domains induced by the external magnetic field was derived from the actual peak widths (see Table 2) at about 105 nm. Further work has to be done to apply this model to other magnetic fluids and to exclude a

**Figure 7**

The S_{hkl} structure factor part extracted from the two-dimensional fit results for different \mathbf{H}_{ext} field directions Ω .

variety of alternative hypotheses, *e.g.* scattering from ordered aggregates. Very recent results (Klokkenburg *et al.*, 2006) with non-scattering methods support the present model.

This project was supported by the German Research Foundation (DFG), project No. Wi 1151/2.

References

- Guinier, A. & Fournet, G. (1955). *Small-Angle Scattering of X-Rays*. New York: John Wiley.
- Heinemann, A., Herrmann, H., Wiedenmann, A., Mattern, N. & Wetzig, K. (2000). *J. Appl. Cryst.* **33**, 1386–1892.
- Heinemann, A. & Wiedenmann, A. (2003). *J. Appl. Cryst.* **36**, 845–849.
- Klokkenburg, M., Erne, B., Meeldijk, J., Wiedenmann, A., Petukov, A., Dullens, R. & Philipse, A. (2006). *Phys. Rev. Lett.* **97**, 185702.
- Pedersen, J. S. (1994). *J. Appl. Cryst.* **27**, 595–608.
- Weisstein, E. W. (1999). *Concise Encyclopedia of Mathematics*. Boca Raton: CRC Press.
- Wiedenmann, A. & Heinemann, A. (2005). *J. Magn. Magn. Mater.* **289**, 58–61.
- Wiedenmann, A., Hoell, A., Kammel, M. & Boesecke, P. (2003). *Phys. Rev. E*, **68**, 031203.